Journal of Applied Mechanics and Technical Physics, Vol. 40, No. 4, 1999

NUMERICAL STUDY OF THE LAMINAR THERMOCAPILLARY FLOW IN A SQUARE CAVITY

V. A. Gaponov

UDC 536.24

The hydrodynamic and heat-transfer processes in the problem of a laminar thermocapillary flow of a viscous incompressible fluid in a square cavity with isothermal vertical and isentropic horizontal surfaces are investigated numerically under the assumption that the gravity is absent, the free surface is flat, and the surface tension depends linearly on the temperature. Calculations were performed by a compact-difference method on irregular grids with a fifth-order accuracy for four Prandtl numbers (Pr = 1, 16, 200, and 3000) *as the Marangoni* (Ma) *number varies from* 10^2 *to* 10^4. *The maximum local heat transfer versus the* Ma *number is obtained. It is shown that, for the* Pr *values considered, the maxima of the distribution of the horizontal velocity component on the surface is displaced to the cold boundary according to a law inversely proportional to the* Ma *number.*

Introduction. Generally, the thermocapillary effect, which occurs at the free boundary of a nonuniformly heated fluid owing to the dependence of the surface-tension coefficient on the temperature (thermocapillary convection), does not show up as a dominating factor in ground conditions but accompanies a more strikingly expressed thermogravity convection, forming the thermal gravitational-capillary convection in combination with it [1–3]. The solution of the problems of thermocapillary convection is complicated by the fact that the value of the velocity along the surface is not known even in the simple case of a flat free surface; there is only a relation between its derivative on the normal to the surface and the derivative along the temperature tangent at the same point. Under these conditions, it is difficult to obtain reliable quantitative data on the local flow and heat-transfer characteristics, which are most important in applied studies; an insufficiently accurate approximation of the boundary conditions at the surface can cause gross errors in local characteristics and affect considerably the general flow pattern.

This study deals with the numerical modeling of thermocapillary convection under conditions in which gravity is absent (the theoretical zero gravity). The hydrodynamics and the heat transfer in the problem of a laminar thermocapillary flow of a viscous incompressible fluid in an open square cavity with isothermal vertical and isentropic horizontal surfaces are studied. It is assumed that the free surface is flat and the surface tension depends linearly on the temperature. The present study is motivated also by the circumstance that the results of [4, 5] and [6, 7] are inconsistent; however, this inconsistency has not yet been eliminated nor even discussed. For example, the distributions of the longitudinal velocity component at an open surface which were obtained for Pr = 1 and their evolution with increase in the Ma number differ significantly already at a qualitative level; the dependence of the flow structure on the Pr number is also interpreted differently.

In the present study, the calculations were performed by a compact-difference method [8, 9] for Pr = 1, 16, 200, and 3000 with variation in the Ma number from 10^2 to 10^4. The method was previously tested on the problem of a two-dimensional flow of a viscous incompressible fluid in a square cavity with a moving lid [9] and on the problem of a convective flow in a closed cavity [10]. The results of [10] allowed one to conclude

Kutateladze Institute of Thermal Physics, Siberian Division, Russian Academy of Sciences, Siberian Division, Russian Academy of Sciences, Novosibirsk 630090. Translated from Prikladnaya Mekhanika i Tekhnicheskaya Fizika, Vol. 40, No. 4, pp. 81–89, July–August, 1999. Original article submitted August 14, 1997.

 0021-8944/99/4004-0622 $22.00

that the proposed method is capable of competing, in accuracy, with spectral methods and is more perfect than the second- and fourth-order finite-difference methods.

Formulation of the Problem. The system of nonlinear equations of the thermocapillary convection in the Oberbeck–Boussinesq approximation, which describes the two-dimensional stationary convective motion of a fluid at zero gravity, can be presented in the following dimensionless form [4]:

$$u\frac{\partial\omega}{\partial x}+v\frac{\partial\omega}{\partial y}=\frac{\mathrm{Pr}}{\mathrm{Ma}}\nabla^2\omega; \tag{1}$$

$$\nabla^2\psi=\omega; \tag{2}$$

$$u\frac{\partial T}{\partial x}+v\frac{\partial T}{\partial y}=\frac{1}{\mathrm{Ma}}\nabla^2 T. \tag{3}$$

Here the stream function $\psi(x,y)$ is introduced by the relations $u=\partial\psi/\partial y$ and $v=-\partial\psi/\partial x$, $\omega(x,y)$ is the velocity vortex determined by the relation $\omega=\partial u/\partial y-\partial v/\partial x$, and $T(x,y)$ is the temperature.

The boundary conditions of the problem that we are interested in have the form

$$\begin{gathered}\psi=\frac{\partial\psi}{\partial x}=0,\quad T=0.5\quad\text{for}\quad x=0,\qquad \psi=\frac{\partial\psi}{\partial x}=0,\quad T=-0.5\quad\text{for}\quad x=1,\\ \psi=\frac{\partial\psi}{\partial y}=0,\quad \frac{\partial T}{\partial y}=0\quad\text{for}\quad y=0,\qquad \psi=0,\quad \frac{\partial^2\psi}{\partial y^2}=-\frac{\partial T}{\partial x},\quad \frac{\partial T}{\partial y}=0\quad\text{for}\quad y=1.\end{gathered} \tag{4}$$

The transition to dimensionless quantities is carried out using the following relations (the dimensional quantities are primed):

$$x=x'/L,\qquad y=y'/L,\qquad \boldsymbol{U}=\boldsymbol{U}'\cdot\left(\frac{L}{a}\frac{1}{\mathrm{Ma}}\right)=\boldsymbol{U}'\cdot\left(\frac{\mu}{\Delta T\sigma_T}\right),$$

$$T=\frac{T'-T_0}{\Delta T},\quad T_0=\frac{T_1+T_2}{2},\quad \Delta T=T_1-T_2,\quad \mathrm{Ma}=\frac{\Delta T\sigma_T L}{\mu a},\quad \mathrm{Pr}=\frac{\nu}{a}.$$

Here L is the side of the square cavity, $\boldsymbol{U}=(u,v)$ is the velocity vector, T_1 and T_2 ($T_1>T_2$) are the temperatures of the hot (left) and cold (right) vertical rigid surfaces of the cavity, respectively, μ is the dynamic viscosity, ν is the kinematic viscosity, a is the thermal diffusivity, and σ_T is the temperature coefficient of surface tension.

Numerical Method. A numerical solution of problem (1)–(4) is obtained by a fifth-order compact-difference method on irregular structured grids [9]. The principle of separate solution of the equations, the method of reaching the steady state, and the method of fractional steps are used.

Compact Difference Approximations. Let there be a quite smooth function of one variable $f(x)$ and $f_k=f(x_k)$, where $k=0,1,\ldots,N$, are its grid values. The compact difference approximations (with a separate approximation of space derivatives) m_k and M_k of the first two derivatives of the function $f(x)$ at the point x_k can be presented in the following operator form [8]:

$$A_x m_k=(1/h_k)B_x f_k,\qquad m_k=L_x f_k,\qquad L_x=(1/h_k)A_x^{-1}B_x,$$

$$A_{xx}M_k=(1/h_k^2)B_{xx}f_k,\qquad M_k=L_{xx}f_k,\qquad L_{xx}=(1/h_k^2)A_{xx}^{-1}B_{xx}.$$

Here $h_k=x_{k+1}-x_k$ for all admissible values of k. The operators A_x, B_x, A_{xx}, and B_{xx} are determined, up to the normalizing factor, by its dimensionless coefficients, which can be directly obtained by various known methods, for example, by the method of undetermined coefficients. Here we use compact differences constructed on a five-point irregular template. They link five values of the function and three values of the first- or second-order derivatives. Eight free parameters allow one to construct sixth-order approximations for the first-order derivative and fifth-order approximations for the second-order derivative. In the particular case of a uniform grid, the constructed approximations have the sixth order of accuracy and are reduced to the

known relations [11]

$$A_x m_k = m_{k-1} + 3m_k + m_{k+1}, \qquad B_x f_k = \frac{1}{12}\{-f_{k-2} - 28f_{k-1} + 28f_{k+1} + f_{k+2}\},$$

$$A_{xx} M_k = 2M_{k-1} + 11M_k + 2M_{k+1}, \qquad B_{xx} f_k = \frac{3}{4}\{f_{k-2} + 16f_{k-1} - 34f_k + 16f_{k+1} + f_{k+2}\}.$$

Transfer Equations. In the case of Eq. (1), the splitting scheme for the transfer equations has the form

$$\frac{2}{\Delta t_1}(\omega^{n+1/4} - \omega^n) + u^n L_x \omega^n + v^n L_y \omega^n = \frac{\mathrm{Pr}}{\mathrm{Ma}}(L_{xx}\omega^{n+1/4} + L_{yy}\omega^n),$$

$$\frac{2}{\Delta t_1}(\omega^{n+1/2} - \omega^n) + u^n L_x \omega^{n+1/4} + v^n L_y \omega^n = \frac{\mathrm{Pr}}{\mathrm{Ma}}(L_{xx}\omega^{n+1/2} + L_{yy}\omega^n),$$

$$\frac{2}{\Delta t_1}(\omega^{n+3/4} - \omega^{n+1/2}) + u^n L_x \omega^{n+1/2} + v^n L_y \omega^n = \frac{\mathrm{Pr}}{\mathrm{Ma}}(L_{xx}\omega^{n+1/2} + L_{yy}\omega^{n+3/4}),$$

$$\frac{2}{\Delta t_1}(\omega^{n+1} - \omega^{n+1/2}) + u^n L_x \omega^{n+1/2} + v^n L_y \omega^{n+3/4} = \frac{\mathrm{Pr}}{\mathrm{Ma}}(L_{xx}\omega^{n+1/2} + L_{yy}\omega^{n+1}).$$

The scheme is conditionally stable and has the first order of approximation in time.

The Poisson equation for the stream function (2) was solved according to the scheme

$$\frac{2}{\Delta t_2}(\psi^{n+1,r+1/2} - \psi^{n+1,r}) = L_{xx}\psi^{n+1,r+1/2} + L_{yy}\psi^{n+1,r} - \omega^{n+1},$$

$$\frac{2}{\Delta t_2}(\psi^{n+1,r+1} - \psi^{n+1,r+1/2}) = L_{xx}\psi^{n+1,r+1/2} + L_{yy}\psi^{n+1,r+1} - \omega^{n+1},$$

where Δt_2 is the step in fictitious time and $t_2 = r\Delta t_2$. The scheme has the second order of approximation in time.

Approximation of the Boundary Conditions. For the velocity vortex on a rigid surface, the approximation was carried out by a fifth-order explicit formula [9] which takes the following form in the case of the lower horizontal surface:

$$\omega_{i,0} = \frac{1}{18h_0^2}(-247\psi_{i,0} + 108\psi_{i,1} + 135\psi_{i,2} + 4\psi_{i,3}) - \frac{1}{3h_0}(20u_{i,0} + 36u_{i,1} + 9u_{i,2}).$$

Here $h_0 = y_1 - y_0$ ($\psi_{i,0} = u_{i,0} = 0$).

In sweeping with a fractional step on the coordinate x, a technique which is conventional for the compact-difference method is used: the half-sum of the approximations corresponding to the nth and $(n+1)$th steps is used as the boundary condition for a velocity vortex.

The presence of the free boundary introduces specifics of its own into the formation of boundary conditions. For example, in a numerical differentiation of the stream function with respect to the coordinate y we used the scheme [9]

$$m_0 + 6m_1 + 3m_2 = \frac{1}{3h_0}(-10f_0 - 9f_1 + 18f_2 + f_3) \qquad (m_0 = 0, \quad f_0 = 0)$$

to determine the velocity component u for a rigid boundary (the cavity bottom) and the scheme

$$17m_{N-2} + 28m_{N-1} = \frac{1}{2h_{N-1}}(-4f_{N-3} - 65f_{N-2} + 52f_{N-1} + 17f_N) - h_{N-1}M_N$$

for an open surface. Here M_N is the second-order derivative of the stream function on the normal to the surface in (4). The desired velocity at the boundary is determined by the scheme

$$m_N = \frac{1}{12h_{N-1}}(-7f_{N-2} - 16f_{N-1} + 23f_N) - \frac{1}{6}(m_{N-2} + 8m_{N-1} - h_{N-1}M_N).$$

Solution of the Grid Equations. The calculations are eventually reduced to a monotone five-diagonal scalar sweep for diffusion terms and a three-diagonal sweep for convective terms. In all cases, the strictly

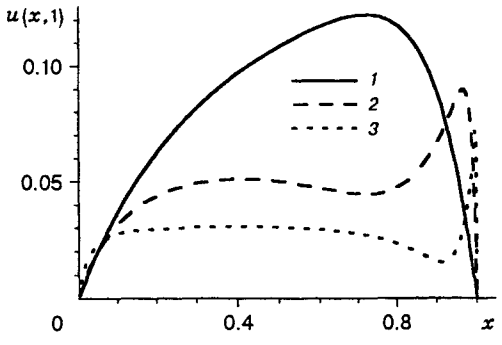

Fig. 1

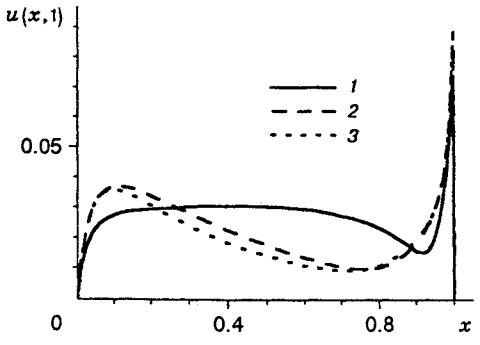

Fig. 2

diagonal dominance takes place. The coefficients of the band matrices formed depend only on the grid parameters and do not change in passing from one time layer to another. This circumstance allows one to avoid multiple factorization of the matrices; the computing resources are spent mainly on the return sweep.

In the calculations, rectangular irregular grids which expand to the center and refine at the boundaries of the region and are uniquely determined by the expansion (concentration) coefficient are employed [9]. For a convenient approximation of the boundary conditions, the three near-boundary intervals on the normal to the boundary were taken to be equal to each other. The grid included 20×20, 40×40 and 60×60 cells. In the latter case, the minimum step along the spatial coordinate decreased to $h_0 = 0.00259$, which corresponds to a 386×386 uniform grid.

For Eqs. (2) and (3), the step over fictitious time was assumed to be constant: $\Delta t_2 = 0.2$ and $\Delta t_3 = 0.1$, respectively. For Eq. (1), the step for $\mathrm{Pr} = 1$ (a 60×60 grid) varied from $\Delta t_1 = 0.0003$ for $\mathrm{Ma} = 10^2$ to $\Delta t_1 = 0.03$ for $\mathrm{Ma} = 10^4$. The iterations terminated when the condition $\max_{i,j} |\omega_{i,j}^{n+1} - \omega_{i,j}^n| / \max_{i,j} |\omega_{i,j}^n| < \varepsilon$ was satisfied. A typical value for ε in the calculations was $\varepsilon = 10^{-7}$. During iterations, in addition to characteristics such as the integral thermal flux in three vertical cross sections of the cavity (in the central cut and on the walls), which are standard for problems of this kind, local characteristics that are most sensitive to the method of approximating the spatial derivatives were monitored. One of them is the temperature derivative $\partial T/\partial x$ at the point with coordinates $(x = 1,\ y = 1)$. After the iterations were completed, the local thermal balance in the cells, which was also calculated by the compact-difference method, was monitored.

Results of the Solution. The integral Nusselt number that corresponds to the vertical cut $x = C$ is denoted by Nu_C:

$$\mathrm{Nu}_C = \int_0^1 \mathrm{Nu}\,(C, y)\, dy, \tag{5}$$

where $\mathrm{Nu}\,(C, y) = \mathrm{Ma}\,(uT) - \partial T/\partial x\big|_{x=C}$. The quantity $\mathrm{Nu}\,(C, y)$ is the local Nusselt number at the point with coordinates (C, y) which is connected with the same vertical cut.

The calculations show that the dependence of the flow structure and the heat transfer on the Pr number when it changes from 1 to 3000 is manifested most strikingly in the interval $1 \leqslant \mathrm{Pr} \leqslant 16$, weakens on the interval $16 \leqslant \mathrm{Pr} \leqslant 200$, and becomes negligible hereinafter: all the values of the flow and heat-transfer characteristics that we are interested in and were obtained numerically for $\mathrm{Pr} = 3000$ and differ from the corresponding values for $\mathrm{Pr} = 200$ in the fourth significant figure; consequently, they were excluded from further consideration.

The solution of the problem is characterized by significant local temperature and velocity gradients on the free surface, which are concentrated near the cold boundary as the Ma number increases. Figures 1–6 give a qualitative idea of the flow structure and indicate the presence of zones with significant temperature and velocity-field gradients and the evolution of the flow structure as the Ma and Pr numbers change. Figure 1 shows the distribution of the horizontal velocity component on the open surface for $\mathrm{Pr} = 1$ and $\mathrm{Ma} = 10^2$

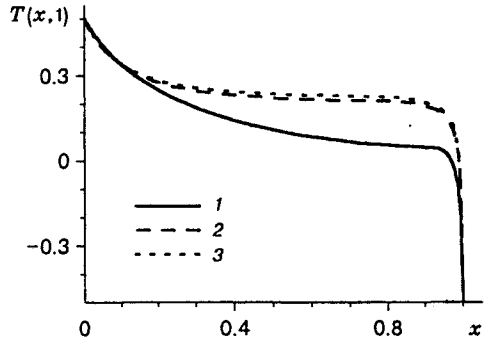

Fig. 3

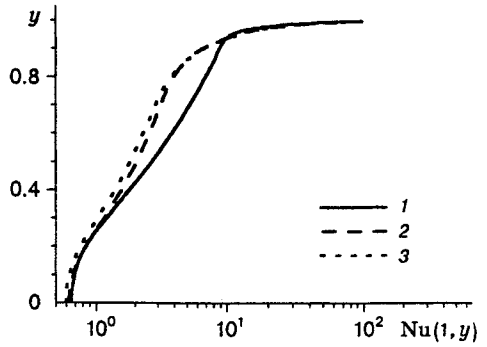

Fig. 4

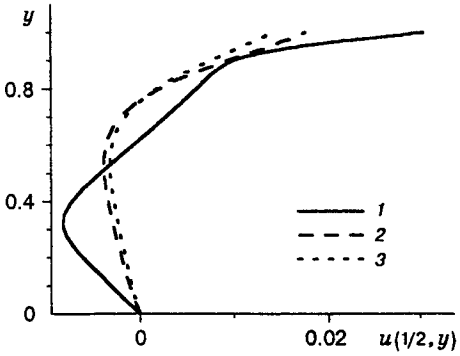

Fig. 5

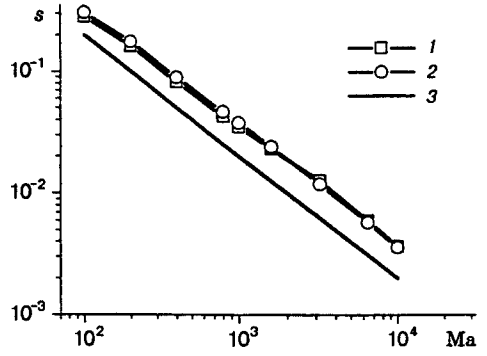

Fig. 6

10^3, and 10^4 (curves 1 and 3). One can see that, as the Ma number increases, the global maximum of the distribution is displaced to the cold boundary (cf. [4]).

We shall trace the evolution of one of the flow regimes shown in Fig. 1 which corresponds to $\mathrm{Ma} = 10^4$ depending on the Pr number (curve 3). Figure 2 demonstrates the distribution of the same velocity component for $\mathrm{Pr} = 1$, 16, and 200 (curves 1–3). Figure 3 shows the temperature distribution on the free surface, Fig. 4 the local heat transfer along the vertical cold boundary, and Fig. 5 the horizontal velocity component in the vertical cut $x = 1/2$ for three flow regimes represented by the velocity distributions in Fig. 2. Figures 3 and 4 indicate the presence of significant temperature gradients in the neighborhood of the point with coordinates $(x, y) = (1, 1)$, where the fluid which moves along the surface and is not yet cooled, runs into the cold wall. The maximum of the local heat transfer is reached at the same point, i.e., $\mathrm{Nu_{max}} = \mathrm{Nu}\,(1, 1)$, for all the Ma and Pr values considered. For adequate graphic representation of the distributions, a logarithmic scale is used.

The local features of the convection heat transfer on vertical walls depend on the flow structure, which is, in turn, determined by the Pr number. For $\mathrm{Pr} = 1$ and $\mathrm{Ma} = 10^2$, the flow is weak and near-surface. With increase in the Ma number, the cooled fluid flow propagates farther and farther along the cold boundary and reaches the cavity bottom (curve 1 in Fig. 5); the center of the main vortex is displaced farther toward the geometric center of the cavity. In this case, as noted in [6], the evolution of the spatial flow structure relative to the Ma number is similar, in many respects, to the evolution of the flow in a cavity with a moving lid. The secondary and tertiary vortices develop in the lower corners of the cavity. The secondary vortices are shaped asymmetrically and evolve according to a complicated law: the right vortex increases monotonically, and the left first decreases in dimensions, reaching the minimum (in the width and height) for $\mathrm{Ma} \approx 3 \cdot 10^3$; after this, its geometrical parameters begin to increase monotonically. The tertiary vortices are shaped more symmetrically (the width is equal to the height within two significant figures); evolving, they repeat the dynamics of the corresponding secondary vortices. It is noteworthy that, in this case, the secondary vortices do not affect the structure of the local convective heat transfer neither on the cold nor hot walls.

TABLE 1

Ma	Grid size	$u(1/2, 1)$	Nu_0	$Nu_{1/2}$	Nu_1	$\omega(0,1)$	$\omega(1,1)$
10^2	20 × 20	$1.0879 \cdot 10^{-1}$	1.0965	1.0965	1.0965	0.7239	2.044
	40 × 40	$1.0869 \cdot 10^{-1}$	1.0962	1.0962	1.0962	0.7300	2.028
	60 × 60	$1.0869 \cdot 10^{-1}$	1.0962	1.0962	1.0962	0.7301	2.028
10^3	20 × 20	$4.9380 \cdot 10^{-2}$	1.9294	1.9269	1.9299	0.9437	12.32
	40 × 40	$5.0007 \cdot 10^{-2}$	1.9259	1.9259	1.9257	0.9545	11.85
	60 × 60	$5.0018 \cdot 10^{-2}$	1.9258	1.9258	1.9258	0.9550	11.75
	64 × 64	—	1.92*	—	1.93*	—	11.8*
	64 × 64	—	—	—	—	1.0**	11.79**
10^4	40 × 40	$2.6855 \cdot 10^{-2}$	4.4099	4.2785	4.4000	2.2124	67.53
	60 × 60	$3.0381 \cdot 10^{-2}$	4.3621	4.3621	4.3654	2.2334	77.09
	64 × 64	—	4.32*	—	4.34*	2.4*	60.2*
	64 × 64	$2.96 \cdot 10^{-2**}$	4.36**	4.33**	4.40**	—	—

Note. One and two asterisks refer to the data from [6] and [7], respectively.

For Pr = 16 and with increase in the Ma number to Ma = 10^4, the flow remains near-surface (curve 2 in Fig. 5), and the center of the vortex is displaced in the direction of the hot wall; in practice, the secondary and tertiary vortices in the lower corners are not changed in dimensions.

An analysis of the structures of the longitudinal velocity component $u(1/2, y)$ for large Ma values and various values of the Pr number shows, that, already for Ma = 10^3, in the case of a high-viscous fluid (Pr $\geqslant$ 16), one can observe an intense surface fluid flow from the hot to the cold wall and a near-surface return compensating (by virtue of the law of mass conservation) flow which affects little the fluid flow in the near-bottom region. The global minimum for $y \approx 0.3$ is observed in a low-viscosity fluid (Pr = 1) on the same velocity profile, i.e., the fluid in the near-bottom region is involved in an intense compensating flow. The indicated position of the extremum on the structure of the longitudinal velocity component is well correlated with the position of the global maximum on the profile of the local convective heat transfer along the hot surface.

Higher-Accuracy Solution. Some flow and heat-transfer characteristics of problem (1)–(4) for Pr = 1, which were borrowed from [6, 7], and the data on the dependence of the solution that we obtained on the grid size used, are given in Table 1. For a more complete quantitative description of the flow considered and with a view to creating the conditions for objective testing of computing schemes, we expand this set of characteristics by introducing the values of the stream function at the center of the cavity, the maximum horizontal velocity component on the open surface, the extrema of the same velocity component in the vertical central cut, the extrema of the vertical velocity component in the horizontal central cut, the dimensions of the secondary and tertiary vortices located in the lower corners of the cavity (H is the width and V is the height; the subscripts L and R refer to the left and right corners, respectively), the value of the velocity vortex at three points chosen on the surface, and the maximum local convective heat transfer on the hot vertical surface. The main characteristics of the solution obtained for Pr = 1 on a 60 × 60 grid are shown in Table 2, where all the located extreme characteristics are put into correspondence with their positions.

Evolution of the Maximum of the Velocity Distribution along an Open Surface. A thorough analysis of the velocity distribution $u(x, 1)$ for various Pr numbers allowed one to reveal the following interesting feature: although the shape of the distribution depends on the Pr number (see Fig. 2), the position of its global maxima s reckoned from the cold boundary changes by a power law $s = c \cdot (\mathrm{Ma})^d$ with $d = -0.96 \approx -1$ as the Ma number increases, i.e., it decreases in an inversely proportional dependence on the Ma value for all the Pr values considered. Figure 6 shows the results of s calculation for Pr = 1 and 16 (curves 1 and 2) and the dependence $s = 20/\mathrm{Ma}$ (curve 3).

Parametric Approximations of the Convective Heat-Transfer Characteristics. The calculation results

TABLE 2

Characteristic	Ma		
	10^2	10^3	10^4
$\psi(1/2,1/2)\cdot 10^3$	−6.005	−2.833	−2.859
$\{u_{\max}(x,1)\cdot 10^2; x\}$	{12.24; 0.721}	{9.021; 0.965}	{7.62; 0.996}
$\{u_{\max}(1/2,y)\cdot 10^2; y\}$	{10.87; 1.0}	{5.002; 1.0}	{3.038; 1.0}
$\{u_{\min}(1/2,y)\cdot 10^3; y\}$	{−21.21; 0.537}	{−9.802; 0.518}	{−8.613; 0.325}
$\{v_{\max}(x,1/2)\cdot 10^3; x\}$	{17.58; 0.230}	{8.111; 0.228}	{7.766; 0.247}
$\{v_{\min}(x,1/2)\cdot 10^3; x\}$	{−20.12; 0.800}	{−9.811; 0.800}	{−11.81; 0.844}
$\{H_L(2); V_L(2)\}\cdot 10^2$	{8.95; 9.07}	{8.60; 8.65}	{10.5; 9.66}
$\{H_R(2); V_R(2)\}\cdot 10^2$	{9.41; 9.64}	{10.7; 11.2}	{23.4; 29.5}
$\{H_L(3); V_L(3)\}\cdot 10^3$	{5.32; 5.32}	{5.07; 5.07}	{6.01; 6.01}
$\{H_R(3); V_R(3)\}\cdot 10^3$	{5.64; 5.65}	{6.55; 6.56}	{15.8; 15.8}
$\omega(0,1)$	0.7301	0.9550	2.233
$\omega(1/2,1)$	0.7368	0.3142	0.2852
$\omega(1,1)$	2.028	11.75	77.09
$\{\mathrm{Nu}_{0,\max}; y\}$	{1.223; 0.322}	{2.168; 0.520}	{5.253; 0.409}
Nu_0	1.096 16	1.9258	4.362
$\mathrm{Nu}_{1/2}$	1.096 16	1.9258	4.362
Nu_1	1.096 16	1.9258	4.365

allow one to construct the parametric approximations of the integral convective heat transfer (Nu_0) and the maximum local convective heat transfer ($\mathrm{Nu}_{\max}$) as a function of the Ma number on the interval $10^3 \leqslant \mathrm{Ma} \leqslant 10^4$:

$$\mathrm{Nu}_0 = 0.17\mathrm{Ma}^{0.35}, \quad \mathrm{Nu}_{\max} = 0.034\mathrm{Ma}^{0.84}, \quad \mathrm{Pr} = 1; \tag{6}$$

$$\mathrm{Nu}_0 = 0.29\mathrm{Ma}^{0.28}, \quad \mathrm{Nu}_{\max} = 0.020\mathrm{Ma}^{0.93}, \quad \mathrm{Pr} = 16; \tag{7}$$

$$\mathrm{Nu}_0 = 0.31\mathrm{Ma}^{0.27}, \quad \mathrm{Nu}_{\max} = 0.013\mathrm{Ma}^{0.98}, \quad \mathrm{Pr} = 200. \tag{8}$$

An analysis of the approximations (6)–(8) results in the following conclusion: a faster increase in $\mathrm{Nu}_{\max}$ corresponds to a larger value of Pr, which affects the exponent of the resulting approximation. It is of interest that this fact is observed against the background of the relative decrease in the integral heat flux through a fluid layer: as the Pr number changes from 1 to 200, the exponent in the approximation $\mathrm{Nu}_{\max}$ increases approximately from 4/5 to 1, whereas the corresponding parameter Nu_0 decreases from 1/3 to 1/4. The directly proportional dependence of $\mathrm{Nu}_{\max}$ on the Ma number correlates with the revealed specifics of the evolution of s; this dependence is manifested more and more strikingly as the Pr number increases (Fig. 6).

Conclusions. The local characteristics of a thermocapillary flow which is characterized by the presence of regions with relatively large local velocity and temperature gradients have been investigated numerically with high spatial resolution. The specifics which is common for all the flows considered (a medium with various values of Pr) has been established based on the calculation results. According to this specifics, the position of the maxima of the horizontal velocity component is displaced to the cold boundary with increase in the Ma number. A large temperature gradient arises near the cold wall (see Figs. 3 and 4); in this connection, the thermocapillary effect acts strongly; the fluid is accelerated, and not only the local but also the global maxima of the horizontal velocity component have been observed. Then a return descending flow is formed, i.e., the slowing down effect of the vertical wall into which the accelerated surface flow of the hot fluid runs into shows up. The local specific feature (the maximum) of the heat flux at the wall is due to this local feature of the flow.

It follows from Table 1 that rough methods (a low-order approximation of spatial derivatives or an insufficiently refined grid) allow one to obtain the integral characteristics (Nu_0 and Nu_1) with acceptable accuracy but result in great errors in determining the local characteristics: $\omega(1,1) \approx 60.2$ [6] is underestimated

by more than 25%. Because the chain of equalities $\omega(1,1) = -\partial T/\partial x\big|_{x=1,y=1} = \mathrm{Nu}(1,1)$ is fulfilled by virtue of (4) and (5), the value of the local convective heat transfer at the contact point of the cold boundary and the open surface is underestimated by more than 25%. A comparison of the integral and local values of the convective heat transfer for Pr = 1 and the approximations constructed on their basis with known results [4, 6] shows that the exponent for $\mathrm{Nu}_{\max}$ in (6) is more than a quarter greater than the value 2/3 given in [6]; the quantity $\mathrm{Nu}_{\max} = 52.1$ that we obtained for Ma = 6400 is more than twice than the corresponding value in [4]. At the same time, both coefficients of the integral convective heat transfer in (6) coincide with the known result within two significant figures [4].

At the same time, Fig. 6 shows that this specifics imposes stringent requirements on the spatial resolution in numerical modeling. The high-accuracy solution given in Table 2 can serve as a test for the finite-difference and second-order finite-element schemes used in numerical modeling of the thermocapillary and thermal gravitational-capillary convections [4–7], for example, in various technological methods of crystal growth.

The author thanks V. S. Berdnikov who attracted the author's attention to the problem for the discussion of the results of numerical modeling.

This work was supported by the Russian Foundation for Fundamental Research (Grant No. 96-01-01499).

REFERENCES

1. S. S. Kutateladze, A. G. Kirdyashkin, and V. S. Berdnikov, "The effect of thermocapillary forces on the transfer processes near the free surface of a fluid in a horizontal layer during turbulent thermal gravitational convection," *Dokl. Akad. Nauk SSSR*, **231**, No. 2, 309–311 (1979).
2. V. S. Berdnikov, "The structure of a freely convective flow of a fluid near a free surface of heat transfer," in: *Problems of Hydrodynamics and Heat Transfer* (collected scientific papers) [in Russian], Inst. of Thermal Phys., Sib. Div., Acad. of Sci. of the USSR, Novosibirsk (1976), pp. 12–22.
3. V. S. Berdnikov, "Thermocapillary convection in a horizontal layer of a fluid," in: *Thermophysical Investigations* (collected scientific papers) [in Russian], Acad. of Sci. of the USSR, Sib. Div., Inst. of Thermal Phys., Novosibirsk (1977), pp. 99–104.
4. V. I. Polezhaev, A. V. Buné, N. A. Verezub, et al., *Mathematical Simulation of Convective Heat Transfer on the Basis of Navier–Stokes Equations* [in Russian], Nauka, Moscow (1987).
5. V. I. Polezhaev, M. S. Bello, N. A. Verezub, et al., *Convective Processes at Zero Gravity* [in Russian], Nauka, Moscow (1991).
6. A. Zebib, G. M. Homsy, and E. Meiburg, "High Marangoni number convection in a square cavity," *Phys. Fluids*, **28**, No. 12, 3467–3476 (1985).
7. V. M. Carpenter and G. M. Homsy, "High Marangoni number convection in a square cavity, Part II," *Phys. Fluids*, **A2**, No. 2, 137–149 (1990).
8. A. I. Tolstykh, *Compact Difference Schemes and Their Application to the Problems of Aerodynamics* [in Russian], Nauka, Moscow (1990).
9. V. A. Gaponov, "Higher-order compact difference approximations in the problems of computing hydrodynamics," Preprint 272-94, Inst. of Thermal Phys., Sib. Div., Russian Acad. of Sci., Novosibirsk (1994).
10. V. A. Gaponov, "Numerical solution of the problem of a convective flow in a closed cavity by the method of higher-order compact differences," Preprint No. 273-94, Thermal Phys., Sib. Div., Russian Acad. of Sci., Novosibirsk (1994).
11. S. K. Lele, "Compact finite difference schemes with spectral-like resolution," *J. Comput. Phys.*, **103**, No. 1, 16–39 (1990).